Inorganic Chemistry

Article

pubs.acs.org/IC

Lanthanide-Thiophene-2,5-dicarboxylate Frameworks: Ionothermal Synthesis, Helical Structures, Photoluminescent Properties, and Single-Crystal-to-Single-Crystal Guest Exchange

Cai-Hong Zhan, Fei Wang, Yao Kang, and Jian Zhang*

State Key Laboratory of Structural Chemistry, Fujian Institute of Research on the Structure of Matter, Chinese Academy of Sciences, Fuzhou, Fujian, 35002, China

Supporting Information

ABSTRACT: Eight three-dimensional lanthanide-thiophene-2,5-dicarboxylate frameworks, $[Ln(TDC)_2]\cdot$(choline) (**1**−**6**; Ln = Gd, Nd, Eu, Er, Tb, Dy; TDC = thiophene-2,5-dicarboxylate), $[Yb(TDC)_2$(e-urea)$]\cdot$(choline)$\cdot H_2O$ (**7**; e-urea = ethyleneurea), $[Nd_2(TDC)_3$(e-urea)$_4]\cdot 3$(e-urea) (**8**) have been successfully prepared in deep eutectic solvents (choline chloride/e-urea), respectively. Compounds **1**−**7** are anionic frameworks with 8-connected **bcu** topology, while compound **8** features a neutral 6-connected **rob**-type framework with guest e-urea molecules. In these structures, lanthanide ions show dicapped trigonal prism, pentagonal bipyramid, and tricapped trigonal prism coordination configurations, respectively, and the TDC ligands exhibit different coordination modes. Versatile helical substructures are presented in these compounds. The photoluminescent properties of compounds **3** (Eu) and **8** (Nd) were studied. Moreover, compound **8** can perform single-crystal-to-single-crystal guest exchange. The ethanol-exchange mechanism of **8** can be ascribed to the kinetically controlled flexibility (KCF).

INTRODUCTION

The synthesis and study of metal−organic frameworks (MOFs) is one of the very active and charming fields in coordination chemistry.[1−3] It has been recognized that MOFs make up the shortages of organic and inorganic components by hybridizing them in an ideal designing way. Through the assembly of organic ligands and metals or metal clusters, a huge variety of MOFs have been obtained. The structure of a MOF is related with many factors, such as charge, coordination geometry, molecular configuration of the ligands, the presence of guest agents, and different experimental conditions etc.[4−6]

There has been a great deal of interest in studying MOFs formed from lanthanide ions.[7−9] The lanthanide (4f) complexes usually show intense emission over narrow wavelength ranges, which are potentially applicable as fluorescent probes and electroluminescent devices.[7] However, lanthanide ions are very poor at absorbing light directly because of the low extinction coefficients of the Laporte forbidden f−f transitions. Energy transfer from an adjacent strongly absorbing chromophore is usually used to stimulate luminescence from lanthanides.[8] Lanthanide MOFs with rich organic ligands as the chromophore groups become an effective solution to make new functional luminescent materials.

Among various types of ligands used to synthesize luminescent MOFs, we choose thiophene-2,5-dicarboxylic acid (H_2TDC) as a sensitizing chromophore and a linker to incorporate lanthanide ions into the hybrid materials. Our consideration is based on the following points: (i) Lanthanide ions are hard acids and preferentially bind to hard (O-donor) atoms.[7] The H_2TDC ligand bearing two carboxylate groups is easy to coordinate with lanthanide ions. (ii) From a structural point of view, H_2TDC seems to be a promising organic linker to construct helical structure, which is widely spread in daily life and in nature, because its two carboxyl groups in a "V-shaped" mode are able to establish bridges through various coordination modes in certain angles.[10] (iii) A lone electron pair of the big S atom in the TDC ligand can be more easily delocalized within the heterocycle, so the ligand can transfer efficiently the energy of the π, π^* excited state to lanthanide ions to increase their luminescence quantum yield. In industry, the H_2TDC ligand is an important intermediate in the preparation of fluorescent brightening agent. Therefore, it is expected that a hybrid lanthanide−TDC compound would have interesting helical structure and photoluminescent property.

Received: September 9, 2011
Published: December 2, 2011

Table 1. Crystal Data and Structure Refinement for 1~8

	1	2	3	4
empirical formula	$C_{17}H_{18}GdNO_9S_2$	$C_{17}H_{18}NdNO_9S_2$	$C_{17}H_{18}EuNO_9S_2$	$C_{17}H_{18}ErNO_9S_2$
formula weight	601.69	588.68	596.40	611.72
crystal system	monoclinic	monoclinic	monoclinic	monoclinic
space group	$P2_1/c$	$P2_1/c$	$P2_1/c$	$P2_1/c$
a (Å)	11.6054(4)	11.6005(3)	11.5776(8)	11.6140(5)
b (Å)	16.2662(5)	16.4488(5)	16.2984(11)	16.0888(7)
c (Å)	12.0479(4)	12.0828(4)	12.0326(9)	12.0204(6)
β (deg)	112.497(2)	112.295(2)	112.500(2)	112.699(2)
V (Å ^{3})	2101.27(12)	2133.21(11)	2097.7(3)	2072.10(16)
Z	4	4	4	4
Dc (g·cm^{-3})	1.902	1.833	1.889	1.961
μ (mm^{-1})	3.404	3.238	3.238	4.301
reflections collected/uniques /Rint	18933/4259/0.0463	8775/2642/0.0704	10396/3666/0.0570	10815/3520/0.0616
S on F^2	1.037	1.020	0.997	0.975
R, wR ($I > 2\sigma(I)$)	0.0328, 0.0648	0.0401, 0.0775	0.0377, 0.0696	0.0364, 0.0734
R, wR (all data)	0.0497, 0.0707	0.0617, 0.0855	0.0599, 0.0776	0.0551, 0.0810
	5	**6**	**7**	**8**
empirical formula	$C_{17}H_{18}TbNO_9S_2$	$C_{17}H_{18}DyNO_9S_2$	$C_{20}H_{10}YbN_3O_{11}S_2$	$C_{39}H_{48}Nd_2N_{14}O_{19}S_3$
formula weight	603.39	606.96	705.47	1401.60
crystal system	monoclinic	monoclinic	monoclinic	monoclinic
space group	$P2_1/c$	$P2_1/c$	$P2_1/c$	$P2/c$
a (Å)	11.6017(2)	11.5408(17)	14.0214(2)	17.3413(5)
b (Å)	16.2188(3)	16.159(2)	11.5047(2)	11.6871(3)
c (Å)	12.0231(2)	12.0019(16)	20.4346(3)	27.8924(10)
β (deg)	112.5710(10)	112.733(6)	129.3750(10)	115.104(3)
V (Å ^{3})	2089.05(6)	2064.3(5)	2548.11(7)	5119.0(3)
Z	4	4	4	4
Dc (g·cm^{-3})	1.918	1.953	1.839	1.819
μ (mm^{-1})	3.635	3.872	3.896	2.217
reflections collected/uniques /Rint	10297/3505/0.0427	16196/3775/0.0212	12771/4518/0.0190	19059/8986/0.0228
S on F^2	1.032	1.065	1.003	1.083
R, wR ($I > 2\sigma(I)$)	0.0317, 0.0649	0.0176, 0.0464	0.0248, 0.0652	0.0369, 0.1064
R, wR (all data)	0.0457, 0.0699	0.0210, 0.0485	0.0274, 0.0669	0.0466, 0.1097

In addition, water molecules existing in MOFs may quench luminescent emission. Compared with traditional experimental methods (hydrothermal or solvothermal), ionothermal synthesis in deep eutectic solvents (DESs) might be a quite good choice.[5] DESs are based on the use of choline chloride with various urea derivatives as solvents, which are not yet well developed in the synthesis of MOFs.[5e,f] Although some lanthanide–TDC compounds have been reported previously, to the best of our knowledge, ionothermal synthesis of lanthanide–TDC frameworks in DESs has not been reported yet.

Herein, we report a series of three-dimensional lanthanide–TDC frameworks: $[Ln(TDC)_2]\cdot$(choline) (**1–6**; Ln = Gd, Nd, Eu, Er, Tb, Dy), $[Yb(TDC)_2$(e-urea)$]\cdot$(choline)$\cdot H_2O$ (**7**; e-urea = ethyleneurea), $[Nd_2(TDC)_3$(e-urea)$_4]\cdot 3$(e-urea) (**8**). Compounds **1–7** are choline-templated anionic frameworks with 8-connected **bcu** topology, while compound **8** features a neutral 6-connected **rob**-type framework with guest e-urea molecules. Versatile helical substructures are presented in these compounds. The photoluminescent properties of compounds **3** (Eu) and **8** (Nd) were studied. Moreover, compound **8** can perform an interesting single-crystal-to-single-crystal guest exchange.

EXPERIMENTAL SECTION

All reagents were purchased commercially and used without further purification. All powder X-ray diffraction (PXRD) analyses were recorded on a Rigaku Dmax2500 diffractometer with Cu Kα radiation (λ = 1.54056 Å), with a step size of 0.05°. Thermal stability studies were carried out on a NETSCHZ STA-449C thermoanalyzer with a heating rate of 10 °C/min under N_2 atmosphere. Fluorescence spectra were measured at room temperature with a HORIBA Jobin-Yvon FluoroMax-4 spectrometer.

Synthesis of $[Ln(TDC)_2]\cdot$(choline) (Ln = Gd, Nd, Eu, Er, Tb, Dy) (1~6). $Ln(NO_3)_3\cdot 6H_2O$ (Ln = Gd, Nd, Eu, Er, Tb, Dy) (0.2 mmol), H_2TDC (0.5 mmol, 0.085 g), 1,4-diazabicyclo[2.2.2]octane (DABCO, 0.5 mmol, 0.056 g), choline chloride (4 mmol, 0.56 g), and ethyleneurea hemihydrate (8 mmol, 1.52 g) were placed in a 20 mL vial. The sample was heated at 120 °C for 6 days and then cooled to room temperature. After the sample was washed with ethanol, the crystals suitable for X-ray analyses were obtained.

Synthesis of $[Yb(TDC)_2$(e-urea)$]\cdot$(choline)$\cdot H_2O$ (7). $Yb(NO_3)_3\cdot 6H_2O$ (0.2 mmol, 0.093 g), H_2TDC (0.5 mmol, 0.085 g), DABCO (0.5 mmol, 0.056 g), choline chloride (4 mmol, 0.56 g), and ethyleneurea hemihydrate (8 mmol, 1.52 g) were placed in a 20 mL vial. The sample was heated at 120 °C for 14 days and then cooled to room temperature. After the sample was washed with ethanol, the crystals suitable for X-ray analyses were obtained.

Synthesis of $[Nd_2(TDC)_3$(e-urea)$_4]\cdot 3$(e-urea) (8). $Nb(NO_3)_3\cdot 6H_2O$ (0.2 mmol, 0.093 g), H_2TDC (0.3 mmol, 0.051 g), DABCO (0.5 mmol, 0.056 g), choline chloride (4 mmol, 0.56 g), and ethyleneurea hemihydrate (8 mmol, 1.52 g) were placed in a 20 mL vial. The sample was heated at 120 °C for 8 days and then cooled to room temperature. After the sample was washed with ethanol, the crystals suitable for X-ray analyses were obtained.

dx.doi.org/10.1021/ic201986m | Inorg. Chem. 2012, 51, 523–530

X-ray Crystallographic Study. The diffraction data for **1**−**8** were collected on a Bruker APXE II diffractometer equipped with a graphite-monochromatized Mo Kα radiation (λ = 0.71073 Å) at 296(2) K. Data intensity was corrected by Lorentz-polarization factors and empirical absorption. The structures were solved by direct methods and expanded with difference Fourier techniques. All non-hydrogen atoms were refined anisotropically; the hydrogen atoms bound to carbon were located by geometrical calculations, and their positions and thermal parameters were fixed during the structure refinement. All calculations were performed using SHELXS-97 and SHELXL-97.[11] Basic information pertaining to crystal parameters and structure refinement for **1**−**8** are summarized in Table 1.

RESULTS AND DISCUSSION

Structures of [Ln(TDC)$_2$]·(choline) (Ln = Gd, Nd, Eu, Er, Tb, Dy) (1∼6). The single-crystal X-ray diffraction analyses showed that compounds **1**∼**6** are isostructural and crystallize in monoclinic symmetry with space group $P2_1/c$. As a representative example, the crystal structure of **1** is described here in detail. In the asymmetric unit of **1**, there are one crystallographically independent Gd^{3+} ion, two TDC ligands, and one free choline cation. Two TDC ligands have two different coordination modes, as shown in Scheme 1a and b:

Scheme 1. Five Coordination Modes of TDC in Compounds 1−8.

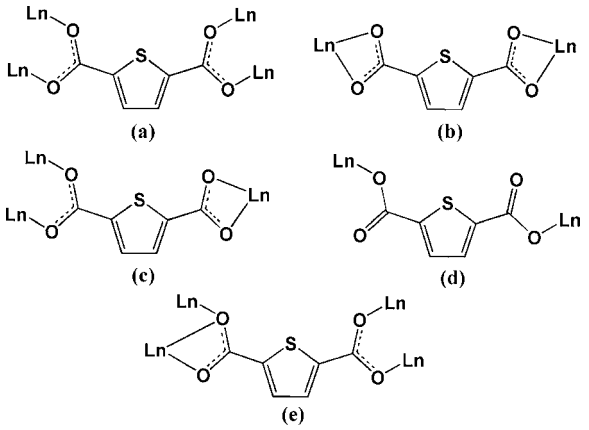

one links four Gd^{3+} ions and another only bridges two Gd^{3+} ions (Figure 1a). Each Gd^{3+} ion is coordinated by eight oxygen atoms from two chelating bidentate carboxylate groups and four μ_2-bridging carboxylate groups, displaying slightly distorted dicapped trigonal prism coordination geometry (Figure 1b). The Gd−O distances range from 2.298(3) to 2.565(3) Å, which are in agreement with those reported Gd complexes. Two identical Gd^{3+} ions are bridged by four carboxylate groups to generate a paddle-wheel $Gd_2(COO)_4$ unit with a Gd· · ·Gd distance of 4.2610(3) Å.

The dinuclear $Gd_2(COO)_4$ subunits are bridged by the μ_4-TDC ligands to form a 2D layer on the *bc* plane, and the adjacent layers are further interconnected by the μ_2-TDC ligands to generate the final 3D framework. It is interesting to note that the framework reveals helical substructures along the *b* axis (Figure 1c). Each helical substructure consists of two left-handed and two right-handed helical chains that are intertwined together (Figure 1d). There are some examples of MOFs with left- and right-handed helical chains. However, most of them are alternately single helical chain. The right- and left-handed helices are arranged equally, so that the whole framework does not show chirality.

Moreover, the framework has large rhombic channels along the *a* axis. The dimension for each channel is about 6.770(4) × 9.061(6) Å (Figure 1f), which is filled by the guest choline cations (Figure 1e). From the viewpoint of structural topology, the whole framework can be topologically represented as a uninodal 8-connected **bcu** network (Schläfli symbol: (4^{24},6^4)) by reducing each dinuclear $Gd_2(COO)_4$ subunit as a 8-connected node (Figure 2a and b).[12]

It is notable that two similar Ln-TDC (Ln = Nd and Eu) compounds have been reported.[10c] They were also prepared under ionothermal conditions, but the ionic liquid used for the synthesis was 1-methyl-3-ethylimidazolium bromide (Emim-Br). So, the Emim cations were captured into the pores of the final **bcu**-type framework. In this work, we used the much cheap deep eutectic solvent (DES) as the ionic liquid for the ionothermal synthesis of six new compounds **1**−**6**. Similar host frameworks with different guest choline cations were generated. These results clearly reveal that the formation of this **bcu**-type framework is not dependent on the type of ionic liquids used. That is truly unusual for such a self-assembly system where the guest cations do not perform a structure-directing role.

Structure of [Yb(TDC)$_2$(e-urea)]·(choline)·H$_2$O (7). Unlike **1**−**6**, compound **7** synthesized under similar ionothermal condition shows a different structure. Although it also crystallized in space group $P2_1/c$, the Yb^{3+} ion in **7** has pentagonal bipyramid coordination geometry (Figure 3b), and the TDC ligands exhibit different coordination modes. In the structure of **7**, each Yb^{3+} ion is coordinated by six oxygen atoms from five TDC ligands and one oxygen atom from one e-urea ligand (Figure 3a). Compared to the structures of **1**−**6**, each Yb^{3+} ion has an additional coordination with the second e-urea ligand. The Yb−O distances range from 2.206(3) to 2.412(3) Å, which are in agreement with those reported Yb complexes. The coordination modes of the TDC ligands are also different from those in **1**−**6**. As shown in Scheme 1c and d, one TDC ligand is a μ3-linker with a monodentate carboxylate group and a didentate carboxylate group, while another is a μ2-linker with two monodentate carboxylate groups. Two identical Yb^{3+} ions are bridged by two carboxyl groups to give a dinuclear unit with a Yb· · ·Yb distance of 5.1943(2) Å (Figure 3a).

The dinuclear {Yb_2} units are bridged by the μ_3-TDC ligands to form a layer, and the resulting layers are further interconnected by the μ_2-TDC ligands to generate the final 3D framework. Different from **1**, there are two kinds of helical substructures along the *b* axis (Figure 3d): (1) the small one is formed from the connectivity between the {Yb_2} units and the μ_3-TDC^{2-} ligands; (2) the large one is based on the connectivity between the {Yb_2} units and both μ_3- and μ_2-TDC ligands. Interestingly, the small helical substructure has alternate right- or left-handedness (Figure 3e), while the large helical substructure comprises two left- and two right-handed helical chains which are intertwined together (Figure 3c). Meanwhile, the right- and left-handed helices are arranged equally, so that the whole framework has no chirality.

Large rhombic channels with the window dimensions of 8.127(5) × 9.555(6)Å are presented in this framework along the *b* axis (Figure 3d). Free choline cations and waters are located in these pores. If each {Yb_2} unit serves for a 8-connected node and each TDC ligand represents a line (Figure 3f),

dx.doi.org/10.1021/ic201986m | Inorg. Chem. 2012, 51, 523−530

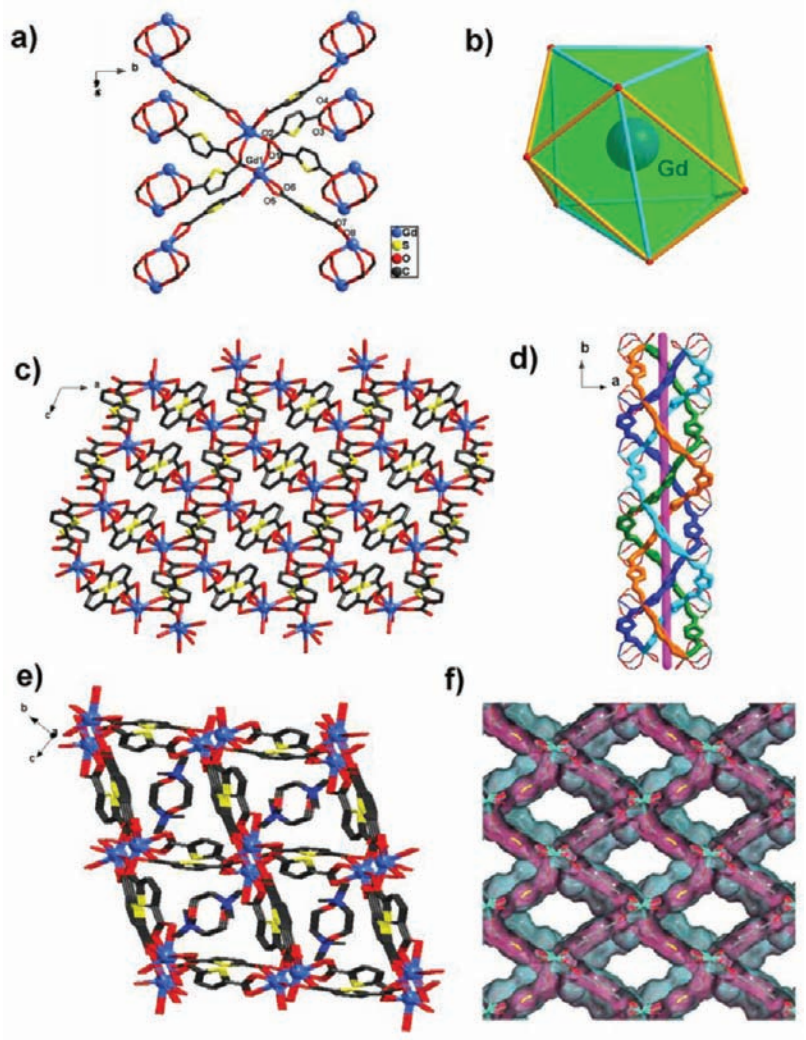

Figure 1. (a) Coordination environment in **1**; (b) distorted dicapped trigonal prism coordination polyhedron of the Gd(III) ion; (c) view of the framework along the *b* axis; (d) two left-handed and two right-handed helical chains intertwined together along the *b* axis; (e) 3D framework of **1** viewed along the approximate *a* axis; (f) rhombic channels in **1**.

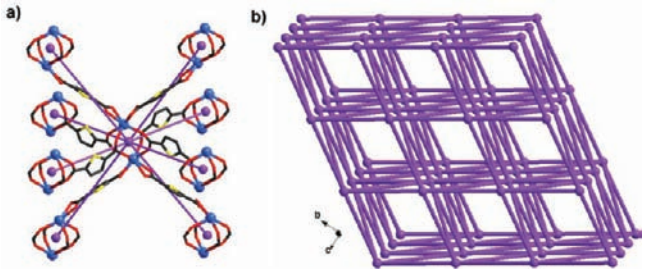

Figure 2. (a) Uninodal 8-connected node represented by the dinuclear unit; (b) **bcu** topology of compound **1**.

the whole framework can also be topologically represented as the 8-connected **bcu** net (Figure 3g).[12]

Structure of $[Nd_2(TDC)_3(e\text{-urea})_4]\cdot 3(e\text{-urea})$ (8). Different from the former seven anionic frameworks (**1**–**7**) that resulted from the ionothermal conditions, compound **8** features a neutral framework with neutral e-urea guest molecules. Compound **8** adopts the same space group $P2_1/c$ and contains similar dinuclear $\{Nd_2\}$ units. In the asymmetric unit of **8**, there are two independent Nd^{3+} ions, three TDC ligands, four terminal e-urea ligands, and three guest e-urea molecules. The TDC ligands exhibit μ_4- and μ_2-coordination modes to link the dinuclear $\{Nd_2\}$ units (Scheme 1b and e). Both independent Nd^{3+} ions are nine-coordinated and have distorted tricapped trigonal prism coordination geometry (Figure 4a and b). Different from **1** to **7**, each Nd^{3+} ion is coordinated by two additional e-urea ligands. The Nd–O distances range from 2.432(4) to 2.803(3) Å. The Nd···Nd distances in the dinuclear $\{Nd_2\}$ unit are 4.1664(3) Å and 4.1022(3) Å, respectively.

The dinuclear $\{Nd_2\}$ units are bridged by the μ_5-TDC ligands to form a layer, and the resulting layers are further interconnected by the μ_2-TDC ligands to generate the final 3D framework of **8** (Figure 4c). Helical substructures are also observed in the structure of **8** along the *b* axis. One helical substructure consists of two left-handed helical chains intertwined together, and another one consists of two right-handed helical chains intertwined together (Figure 4d). Because of the equal ratio between the right- and left-handed helices, the whole structure does not show chirality. The framework only shows small rectangle pores with the dimensions of 3.784(2) × 5.534(1) Å because of the blocking of the coordinated e-urea molecules (Figure 4c). The guest e-urea molecules are located in these pores. Similar to the above topological analysis, each $\{Nd_2\}$ unit serves for a

dx.doi.org/10.1021/ic201986m | *Inorg. Chem.* 2012, 51, 523–530

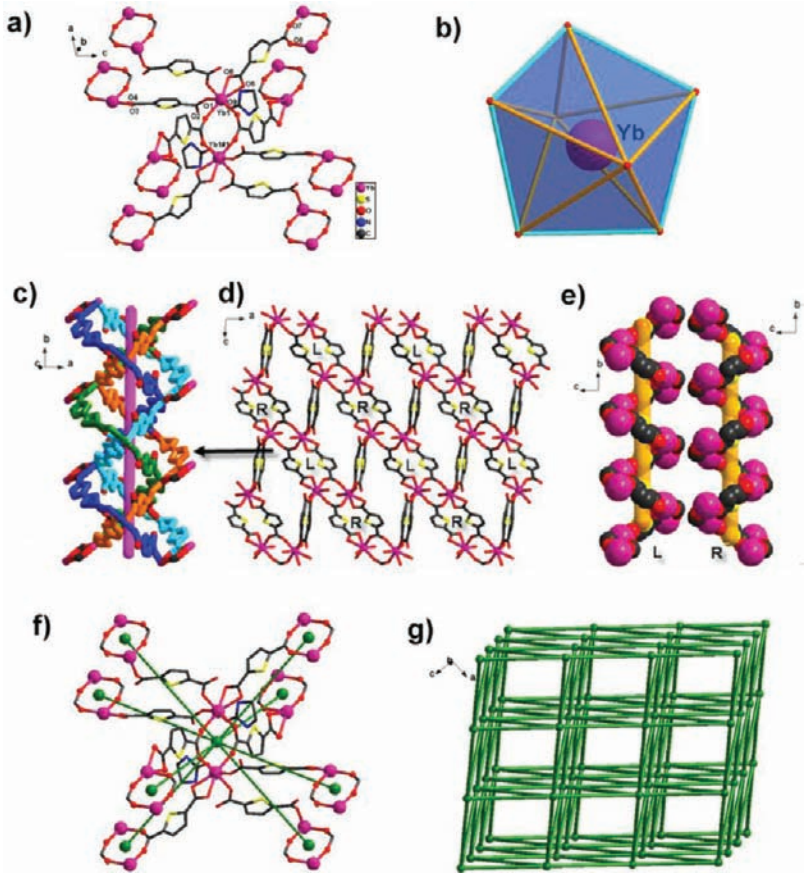

Figure 3. (a) Coordination environment in **7**; (b) distorted pentagonal bipyramid coordination polyhedron of the Yb^{3+} ion; (c) two left- and two right-handed helical chains intertwined together along the *b* axis; (d) view of the framework along the *b* axis; (e) left- and right-handed helices alternatively along the *b* axis; (f) uninodal 8-connected nodes represented by $\{Yb_2\}$ units; (g) **bcu** topology of **7**.

6-connected node and each TDC ligand represents a line (Figure 4e); the whole framework can be topologically represented as a uninodal 6-connected **rob** net with a Schläfli symbol of $(4^8,6^6,8)$ (Figure 4f).[12]

Photoluminescent Properties. H_2TDC ligand has a composition of sensitizing groups and the appropriate energy level, so that it can act as a good sensitizer for the central lanthanide ion. The solid-state photoluminescent properties of compounds **3** and **8** have been measured with excitation wavelength at 350 nm at room temperature (Figure 5). The spectrum of **3** exhibits strong characteristic emissions for Eu(III) ions in the visible region. The emission peaks occurring at 592, 613, 650, and 700 nm can be assigned to $^5D_0 \rightarrow {}^7F_J$ (J = 1−4) transitions, respectively.[14] The symmetric forbidden emission $^5D_0 \rightarrow {}^7F_0$ at 579 nm is a weak band. The most intense emission at 613 nm with a splitting is attributed to the electric dipole induced $^5D_0 \rightarrow {}^7F_2$ transition, which is hypersensitive to the coordination environment of the Eu(III) ions and implies a red emission light of **3**. The medium-strong emission at 592 nm is corresponding to the magnetic dipole induced $^5D_0 \rightarrow {}^7F_1$ transition, which is fairly insensitive to the environment of the Eu(III) ions. A peak is observed for the $^5D_0 \rightarrow {}^7F_3$ transition with weak but measurable intensities, while the $^5D_0 \rightarrow {}^7F_4$ transition comprised of two peaks with not well-defined character. For Eu(III), the splitting of the ground-state levels can be readily predicted from group theory and can allow for the local site symmetry of the compound to be determined. When Eu(III) cations exist in a D_4 site symmetry, two components of the $^5D_0 \rightarrow {}^7F_1$ transition and one component of the $^5D_0 \rightarrow {}^7F_2$ transition are expected to be observed while the $^5D_0 \rightarrow {}^7F_0$ transitions remain strongly forbidden. In fact, **3** shows that only one peak is observed for the $^5D_0 \rightarrow {}^7F_1$ transition, while two peaks are seen on the hypersensitive $^5D_0 \rightarrow {}^7F_2$ transition, indicating a heavy distortion from an ideal D_4 symmetry. The observed $^5D_0 \rightarrow {}^7F_3$ and $^5D_0 \rightarrow {}^7F_5$ transitions also did not show the two distinct peaks expected for an ideal D_4 symmetric Eu(III) ion. In particular, the ratio of the intensities of the $(^5D_0 \rightarrow {}^7F_2)/(^5D_0 \rightarrow {}^7F_1)$ transitions is very sensitive to the symmetry of the Eu(III) centers. Because the $^7F_2$ electric dipole transition is hypersensitive to the ligand environment while the $^7F_1$ magnetic dipole is nearly completely insensitive, it is possible to discern some symmetry elements of a framework, even in the absence of single-crystal X-ray data. The intensity ratio of 5.18 for $I(^5D_0 \rightarrow {}^7F_2)/I(^5D_0 \rightarrow {}^7F_1)$ in **3** further indicates that the symmetry of Eu(III) ion site is low and Eu(III) ions are all not located at the inversion center, which is in good agreement with the result of single-crystal X-ray analysis.

Unlike the emission spectra of **3**, that of **8** exhibits no characteristic luminescence in the visible region, but it shows blue photoluminescence with an emission maximum at 438 nm. The free ligand H_2TDC displays emission band at 477 nm in the visible range, and the photoluminescent intensity of **8** is much stronger than those of the corresponding free ligands. Such a fact indicates that the photoluminescent mechanism of **8** is significantly different from the free ligand. In **8**, the HOMO is associated with the π-bonding orbital from the aromatic ring

dx.doi.org/10.1021/ic201986m | *Inorg. Chem.* 2012, 51, 523−530

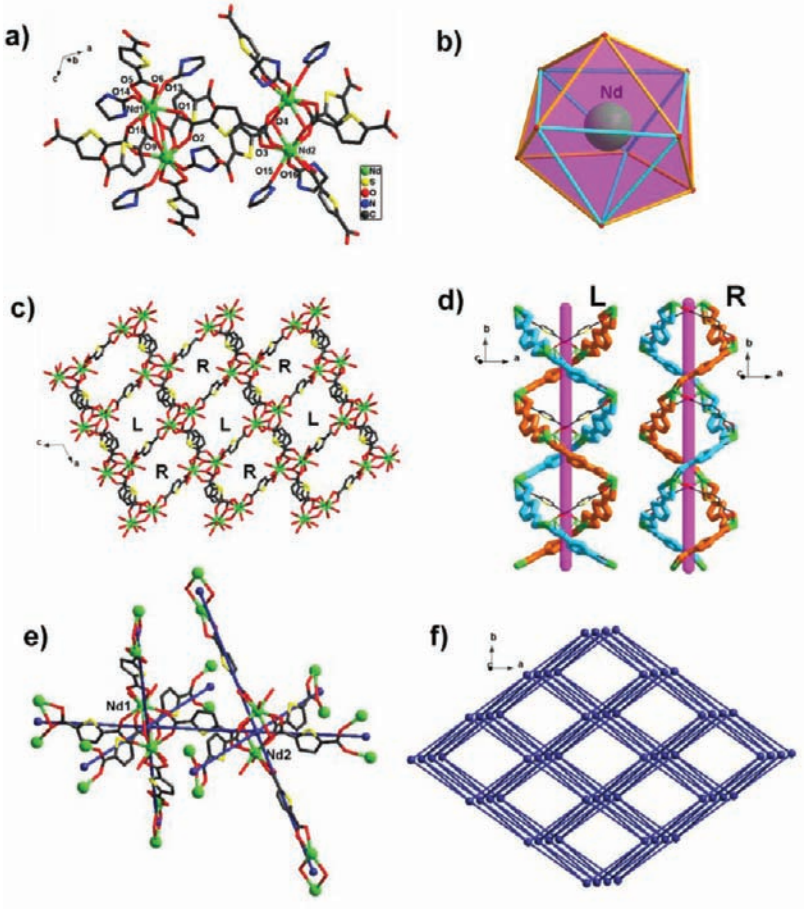

Figure 4. (a) Coordination environment in **8**; (b) distorted dicapped trigonal prism coordination polyhedron of the Nd(III) ion; (c) view of the framework along the *b* axis; (d) two left- and two right-handed helices alternatively along the *b* axis; (e) uninodal 6-connected nodes represented by $\{Nd_2\}$ units; (f) the **rob** topology of **8**.

of ligand, whereas the LUMO may be associated with Nd−O (carboxy) σ^*-antibonding orbital, localized more on the metal centers, similar to the previously reported results. The luminescence band at 438 nm of **8** may be assigned to $\pi \rightarrow 4f$ ligand-to-metal charge transfer (LMCT) transition, and the enhancement of luminescent intensity in **8** may be attributed to the rigid enhancement of the ligands, as a result of coordination to metal ions, and thus reduces the loss of energy through a radiation less pathway.

The mechanism of energy transfer from ligands to metal ions has been widely discussed to interpret the luminescence of lanthanide compounds. When the triplet state energy of the ligand is greater than that of the energy gap between the excited-state and ground-state of the metal ions, efficient luminescence could be obtained. From the results discussed above, we could presume that there is an optimal energy difference between the linker triplet state and the resonant emissive lanthanoid energy level, and here, the optimum energy for Eu(III) seems to have been exceeded, although not for Nd(III).

Thermal Analyses. To study the stability of compounds **3** and **8**, thermogravimetric analysis (TGA) studies were performed. The phase purity of both compounds was characterized using powder X-ray diffraction (Figure S1 in the Supporting Information). For **3**, The TGA curve exhibits two steps of weight losses (Figure S2 in the Supporting Information). The weight loss from 180 to 337 °C corresponds to the release of free choline cations. The observed weight loss of 17.2% is in agreement with the calculated value of 17.5%. The second weight loss, between 337 and 570 °C, is attributable to the loss of TDC ligands. For **8**, The TGA curve exhibits three steps of weight losses, the weight loss from 184 to 255 °C corresponds to the release of free e-urea molecules. The observed weight loss of 18.1% is in agreement with the calculated value of 18.4%. The second weight loss, between 255 and 376 °C, is attributable to the loss of terminal e-urea ligands. The third weight loss, between 376 and 536 °C, belongs to the loss of TDC ligands.

Single-Crystal-to-Single-Crystal Guest Exchange. Direct structural information of the immersed crystals is fundamental to understanding the mechanism of guest molecule exchange. As a result of the weak host−guest interaction, which is unstable in most solvents for mass crystals, the crystal structure determination of the guest-exchanged phases remains a great challenge.[13] In our experiment, for the first time, a sequential process of guest molecule exchange between e-urea and ethanol molecules was captured by analysis of the relevant crystal structures.

In the structure of **8**, there are three kinds of guest e-urea molecules (A, B, and C in Figure 6a). The e-urea A forms strong hydrogen bonds with the host framework; the e-urea B also has normal hydrogen bonding interactions with the host framework, whereas the e-urea C only has weak interactions with the host framework. Thus, we could estimate that e-urea A

dx.doi.org/10.1021/ic201986m | *Inorg. Chem.* 2012, 51, 523−530

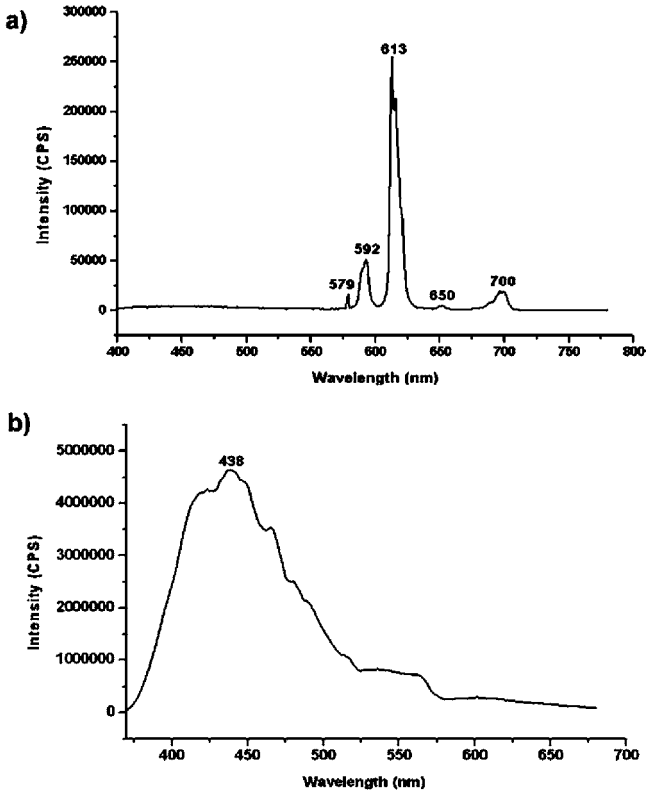

Figure 5. Emission spectra of **3** (a) and **8** (b).

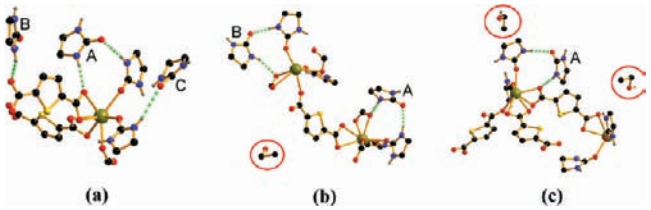

Figure 6. (a) Three kinds of e-ureas in **8** (A, B, and C); (b) e-urea C exchanged by ethanol in **8a**. (c) e-urea B and C exchanged by ethanol in **8b**.

is quite stable, e-urea B is less stable, and e-urea C is not stable. Exactly as we expected, when a single crystal of **8** was immersed in ethanol after 5 h, a new **8a** with two e-urea and one ethanol molecules in each asymmetric unit was obtained. The e-ureas C in **8** are all exchanged by ethanol molecules (Figure 6b). Furthermore, after 3 days, another **8b** with one e-urea and two ethanol molecules in each asymmetric unit was obtained. Both e-urea B and C in **8** are all exchanged by ethanol molecules (Figure 6c). Small framework distortions are also observed (Table S2 in the Supporting Information). For **8a**, it is a 2.1% and 0.6% contraction in the *a*-axis and *c*-axis, respectively, and a 4.2% expansion in the *b*-axis. For **8b**, it is a 1.9% and 1.3% contraction in the *a*-axis and *c*-axis, respectively, and a 3.9% expansion in the *b*-axis. The comparable results reveal that the guest molecule exchanges induce an anisotropic deviation, especially leading to a stretch in some degree along the *b*-axis, which is in agreement with the result that, in the *b* direction, the screw pitch is 24.3598(12) Å in **8a** (4.2% expansion) and 24.2910(15) Å in **8b** (3.9% expansion), compared with 23.3742(7) Å in **8**. The reason may be that the hydrogen bonds are weakened along with ethanol molecules in the structure in the *b*-axis. The ethanol-exchanged **8a** and **8b** are isostructural to the unexchanged one, precluding the occurrence of thermodynamic bistability during the exchange process. Therefore, the ethanol-exchange mechanism of **8** can be ascribed to the kinetically controlled flexibility (KCF) originated from the momentary rotation/swing motions of the e-urea molecules.

Until now, we have not yet got the crystal structure whose guest e-urea molecules are wholly exchanged by ethanol, because the single crystals fracture into microcrystalline powders (**8c**) and turn nontransparent after steeped for a long time. To elucidate the guest exchange mechanism, we also soak **8** in methanol and acetone. Noticeably, the single crystals that immerged in methanol have a high tendency to become nontransparent, while acetone does not induce guest molecule exchanges by single-crystal structure determination. These phenomena may be correlated to the degree of polarity of the solvents. The polar methanol molecules may easily ruin the framework by strong interactions, while nonpolar acetone molecules may show weak impact with the framework and cannot be held in pores.

To ensure the structures of **8a** and **8b**, XRPD and TGA were also measured, as shown in Figure 7. The peak positions of **8**, **8a**, and **8b** are in good agreement, indicating the identical frameworks of **8**, **8a**, and **8b** (Figure 7a). TGA studies show that at the first step, the weight loss from 30 to 95 °C, corresponds to the release of one free ethanol molecule (found, 3.05%; calcd, 3.16%) for **8a**, and two ethanol molecules (found,

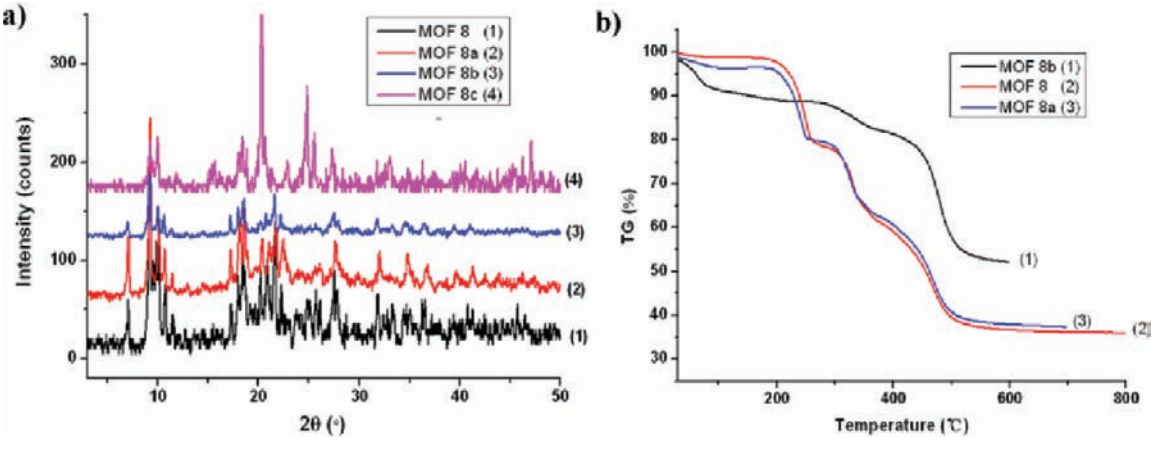

Figure 7. (a) XRPD spectra of **8**, **8a**, **8b**, and **8c**. (b) TGA curves of **8**, **8a**, and **8b**.

dx.doi.org/10.1021/ic201986m | *Inorg. Chem.* 2012, 51, 523–530

6.84%; calcd, 6.97%) for **8b**, which is quite consistent with the structures of **8a** and **8b** (Figure 7b).

CONCLUSION

In conclusion, eight unique 3D Ln-TDC frameworks have been successfully synthesized in deep eutectic solvents. The TDC ligands exhibit different coordination modes in the eight compounds, and versatile helical substructures are observed in the structures. The structural topology analysis identified that **1**∼**7** belong to 8-connected **bcu** net and **8** has 6-connected **rob** net. The studies of the luminescence property exhibit that compound **3** (Eu) has characteristic luminescence in visible region. The most interesting point is that compound **8** can perform single-crystal-to-single-crystal guest exchange. The ethanol-exchange mechanism of **8** is ascribed to the kinetically controlled flexibility (KCF), originated from the momentary rotation/swing motions of the e-urea molecules.

ASSOCIATED CONTENT

Supporting Information

Additional tables, TGA, powder X-ray diffraction patterns, and CIF file. This material is available free of charge via the Internet at http://pubs.acs.org.

AUTHOR INFORMATION

Corresponding Author

*Fax: (+86)-591-83714946. Tel: (+86)-591-83715030. E-mail: zhj@fjirsm.ac.cn.

ACKNOWLEDGMENTS

This work is supported by National Basic Research Program of China (973 Programs 2011CB932504 and 2012CB821705), NSFC (21073191, 21103189, and 21173224), NSF of Fujian Province (2011J06005, 2010J05039), and the Innovation Program of CAS (KJCX2-YW-H21).

REFERENCES

(1) (a) Férey, G. *Chem. Soc. Rev.* **2008**, *37*, 191. (b) Batten, S. R.; Neville, S. M.; Turner, D. R. *Coordination Polymers: Design, Analysis, and Application*; Royal Society of Chemistry: Cambridge, U.K., 2008.

(2) (a) Long, J. R.; Yaghi, O. M. *Chem. Soc. Rev.* **2009**, *38*, 1213. (b) Yang, S.; Lin, X.; Blake, A. J.; Walker, G.; Hubberstey, P.; Champness, N. R.; Schröder, M. *Nat. Chem.* **2009**, *1*, 487. (c) Ma, L.; Lin, W. *Angew. Chem., Int. Ed.* **2009**, *48*, 3637. (d) Zeng, M.-H.; Wang, Q.-X.; Tan, Y.-X.; Hu, S.; Zhao, H.-X.; Long, L.-S. *J. Am. Chem. Soc.* **2010**, *132*, 2561.

(3) (a) Lee, C. S.; Wang, S. L.; Lii, K. H. *J. Am. Chem. Soc.* **2009**, *131*, 15116. (b) Yang, Y. C.; Wang, S. L. *J. Am. Chem. Soc.* **2008**, *130*, 1146. (c) Chen, Y. B.; Kang, Y.; Zhang, J. *Chem. Commun.* **2010**, *46*, 3182. (d) Liu, Y.; Boey, F.; Lao, L. L.; Zhang, H.; Liu, X.; Zhang, Q. *Chem.—Asian J.* **2011**, *6*, 1004.

(4) (a) Zheng, S.; Li, Y.; Wu, T.; Nieto, R.; Feng, P.; Bu, X. *Chem.—Eur. J.* **2010**, *16*, 13035. (b) Chen, S.; Zhang, J.; Wu, T.; Feng, P.; Bu, X. *J. Am. Chem. Soc.* **2009**, *131*, 16027.

(5) (a) Jhang, P. C.; Yang, Y. C.; Lai, Y. C.; Liu, W. R.; Wang, S. L. *Angew. Chem., Int. Ed.* **2009**, *48*, 742. (b) Parnham, E. R.; Morris, R. E. *Acc. Chem. Res.* **2007**, *40*, 1005. (c) Lin, Z.; Wragg, D. S.; Morris, R. E. *Chem. Commun.* **2006**, 2021. (d) Morris, R. E. *Chem. Commun.* **2009**, 2990. (e) Zhang, J.; Wu, T.; Chen, S.; Feng, P.; Bu, X. *Angew. Chem., Int. Ed.* **2009**, *48*, 3486. (f) Chen, S.; Zhang, J.; Wu, T.; Feng, P.; Bu, X. *Dalton Trans.* **2010**, *39*, 697. (g) Zhang, J.; Chen, S.; Bu, X. *Angew. Chem., Int. Ed.* **2008**, *47*, 5434.

(6) (a) Zhang, J.; Chen, S.; Wu, T.; Zheng, S. T.; Chen, Y.; Nieto, R. A.; Feng, P.; Bu, X. *Angew. Chem., Int. Ed.* **2010**, *49*, 8876. (b) Zhang, H. X.; Wang, F.; Yang, H.; Tan, Y. X.; Zhang, J.; Bu, X. *J. Am. Chem. Soc.* **2011**, *133*, 11884. (c) Wang, F.; Liu, Z. S.; Yang, H.; Tan, Y. X.; Zhang, J. *Angew. Chem., Int. Ed.* **2011**, *50*, 450.

(7) (a) Mao, J. G. *Coord. Chem. Rev.* **2007**, *251*, 1493. (b) Bunzli, J. C. G.; Piguet, C. *Chem. Soc. Rev.* **2005**, *34*, 1048. (c) Wang, C. M.; Wu, Y. Y.; Chang, Y. W.; Lii, K. H. *Chem. Mater.* **2008**, *20*, 2857.

(8) (a) Dong, Y. B.; Wang, P.; Ma, J. P.; Zhao, X. X.; Wang, H. Y.; Tang, B.; Huang, R. Q. *J. Am. Chem. Soc.* **2007**, *129*, 4872. (b) Przychodzen, P.; Pelka, R.; Lewinski, K.; Supel, J.; Rams, M.; Tomala, K.; Sieklucka, B. *Inorg. Chem.* **2007**, *46*, 8924. (c) Yue, Q.; Yang, J.; Li, G. H.; Li, G. D.; Chen, J. S. *Inorg. Chem.* **2006**, *45*, 4431. (d) Lu, W.-G.; Jiang, L.; Lu, T.-B. *Cryst. Growth Des.* **2010**, *10*, 4310. (e) Zhuang, G.-L.; Kong, X.-J.; Long, L.-S.; Huang, R.-B.; Zheng, L.-S. *CrystEngComm* **2010**, *12*, 2691. (f) Allendorf, M. D.; Bauer, C. A.; Bhakta, R. K.; Houk, R. J. T. *Chem. Soc. Rev.* **2009**, *38*, 1330.

(9) (a) Nishiyabu, R.; Hashimoto, N.; Cho, T.; Watanabe, K.; Yasunaga, T.; Endo, A.; Kaneko, K.; Niidome, T.; Murata, M.; Adachi, C.; Katayama, Y.; Hashizume, M.; Kimizuka, N. *J. Am. Chem. Soc.* **2009**, *131*, 2151. (b) Mohapatra, S.; Hembram, K.; Waghmare, U.; Maji, T. K. *Chem. Mater.* **2009**, *21*, 5406. (c) Xu, J.; Su, W.; Hong, M. *Cryst. Growth Des.* **2011**, *11*, 337.

(10) (a) Huang, W.; Wu, D.; Zhou, P.; Yan, W.; Guo, D.; Duan, C.; Meng, Q. *Cryst. Growth Des.* **2009**, *9*, 1361. (b) Xu, J.; Cheng, J. W.; Su, W.; Hong, M. *Cryst. Growth Des.* **2011**, *11*, 2294. (c) Wang, M.-X.; Long, L.-S.; Huang, R.-B.; Zheng, L.-S. *Chem. Commun.* **2011**, *47*, 9834.

(11) Sheldrick, G. M. *SHELXS-97*, Program for X-ray Crystal Structure Solution; Göttingen University: Göttingen, Germany, 1997.

(12) (a) Blatov, V. A.; Shevchenko, A. P.; Serezhkin, V. N. *J. Appl. Crystallogr.* **2000**, *33*, 1193. (b) *TOPOS*; Available online: http://www.topos.ssu.samara.ru.

(13) (a) Kitagawa, S.; Uemura, K. *Chem. Soc. Rev.* **2005**, *34*, 109. (b) Rather, B.; Zaworotko, M. J. *Chem. Commun.* **2003**, 830. (c) Mir, M. H.; Vittal, J. J. *Cryst. Growth Des.* **2008**, *8*, 1478.

(14) Datcu, A.; Roques, N.; Jubera, V.; Imaz, I.; Maspoch, D.; Sutter, J.-P.; Rovira, C.; Veciana, J. *Chem.—Eur. J.* **2011**, *17*, 3644.